

---

# CONDITION WEAVING MEETS EXPERT MODULATION: TOWARDS UNIVERSAL AND CONTROLLABLE IMAGE GENERATION

---

**Guoqing Zhang**

Beijing Jiaotong University  
SenseTime Research

**Xingtong Ge**

Hong Kong University of Science and Technology  
SenseTime Research

**Lu Shi**

Beijing Jiaotong University

**Xin Zhang**

SenseTime Research

**Muqing Xue**

Beijing Jiaotong University

**Wanru Xu**

Beijing Jiaotong University

**Yigang Cen \***

Beijing Jiaotong University

## ABSTRACT

The image-to-image generation task aims to produce controllable images by leveraging conditional inputs and prompt instructions. However, existing methods often train separate control branches for each type of condition, leading to redundant model structures and inefficient use of computational resources. To address this, we propose a **Unified image-to-image Generation (UniGen)** framework that supports diverse conditional inputs while enhancing generation efficiency and expressiveness. Specifically, to tackle the widely existing parameter redundancy and computational inefficiency in controllable conditional generation architectures, we propose the **Condition Modulated Expert (CoMoE)** module. This module aggregates semantically similar patch features and assigns them to dedicated expert modules for visual representation and conditional modeling. By enabling independent modeling of foreground features under different conditions, CoMoE effectively mitigates feature entanglement and redundant computation in multi-condition scenarios. Furthermore, to bridge the information gap between the backbone and control branches, we propose **WeaveNet**, a dynamic, snake-like connection mechanism that enables effective interaction between global text-level control from the backbone and fine-grained control from conditional branches. Extensive experiments on the Subjects-200K and MultiGen-20M datasets across various conditional image generation tasks demonstrate that our method consistently achieves state-of-the-art performance, validating its advantages in both versatility and effectiveness. The code has been uploaded to <https://github.com/gavin-gqzhang/UniGen>.

## 1 Introduction

With the continuous advancement of diffusion-based methods [1, 2, 3, 4, 5], model architectures have evolved from the early UNet [6, 1] design to the more recent DiT [7] structure, leading to significant improvements in the quality of synthesized images, particularly in text-guided image generation tasks. However, relying solely on text-to-image generation often fails to meet the requirements for controllable synthesis in scenarios demanding precise spatial or structural guidance. To address this limitation, image-to-image generation based on conditional visual constraints has emerged as another important branch of image synthesis. This task aims to generate images under spatial constraints using various conditional inputs, such as depth, canny, and pose information, etc.

To tackle this task, ControlNet [8] introduces a separate branch to inject spatial condition information into the generation process. IP-Adapter [9] incorporates an adapter structure to enable partial parameter tuning while enforcing spatial constraints. Subsequently, several works [10, 11] have explored approaches inspired by mixture-of-experts (MoE) architectures to handle diverse types of visual conditions. More recently, with the rapid development of the FLUX [5] model in image synthesis, a number of studies [12, 13, 14] have adopted lightweight fine-tuning techniques such as LoRA [15] to enhance spatial constraint capabilities from conditional images by tuning only a subset of model parameters.

---

\*Corresponding author.

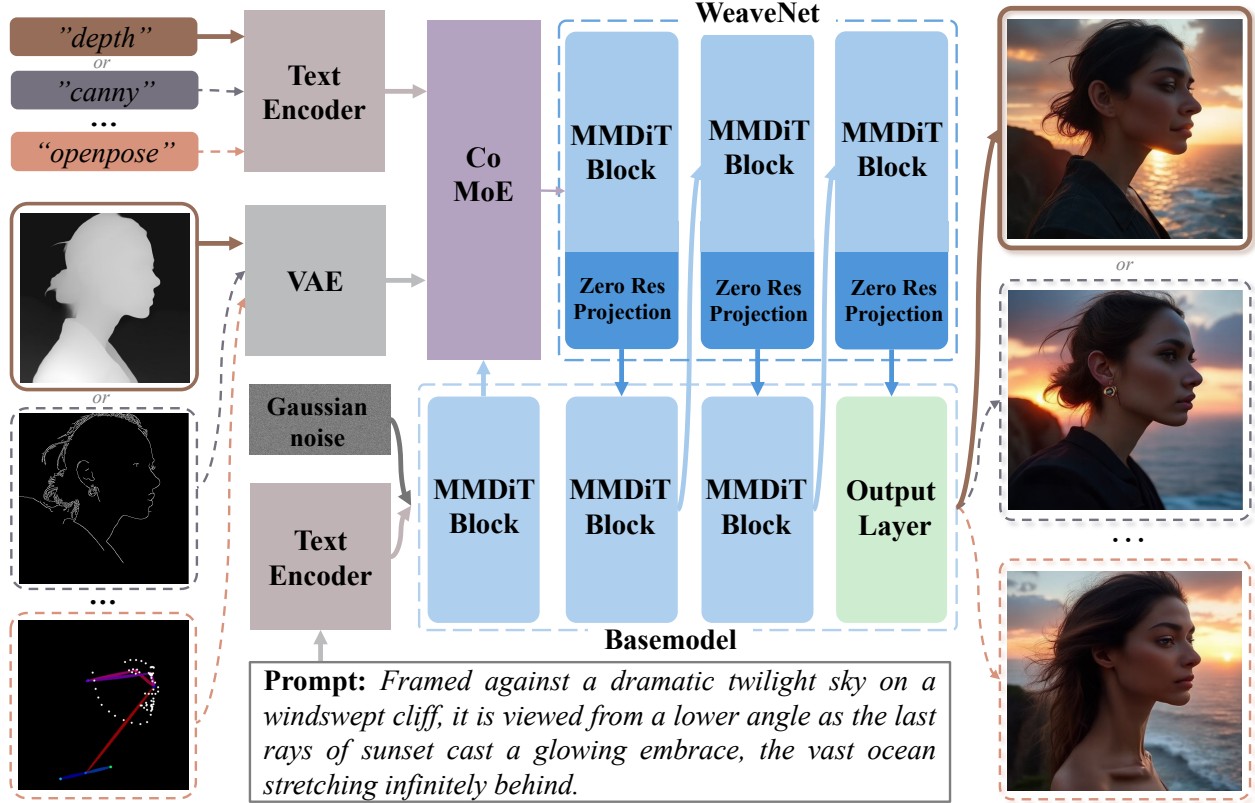


Figure 1: The UniGen architecture supports image inputs with arbitrary types of conditioning to control the content of image generation.

However, existing methods—whether through constructing MoE architectures or introducing additional parameter tuning—typically design independent control units or control branches for each conditional visual input. Therefore, two major limitations remain in diverse conditional image generation tasks: **Firstly, redundant parameters and inefficient computation.** On one hand, some approaches build independent and parallel control units for each condition, leading to significant parameter redundancy. On the other hand, certain methods adopt MoE-like designs that merely select specific preprocessing modules based on the condition type, which substantially differs from mixture-of-experts architectures designed for efficient parallel computation. These strategies overlook both the significant differences and the potential commonalities among conditions, heavily relying on condition-specific modules. This leads to excessive parameter redundancy and inefficient computation, ultimately limiting the model’s practicality. **Secondly, a lack of effective interaction between the global visual representations guided by text and the local visual representations guided by conditional images.** Existing methods typically rely on isolated conditional control modules to extract conditional visual representations, failing to exploit the dynamic interplay between prompt-guided global (holistic) features and condition-image-guided local (spatial) features. This lack of interaction introduces semantic discrepancies between global and local visual cues, often leading to visually abrupt or inconsistent synthesis results.

To address the above challenges, we propose a unified image generation framework, as illustrated in Fig. 1. Firstly, to address the significant computational redundancy caused by existing methods that employ separate modules or branches for processing different conditional visual representations, we propose the Condition Modulated Expert (CoMoE) module. This method starts by analyzing the differences and commonalities among various types of conditional visual representations. It aggregates patch features from conditional visual inputs into foreground and background regions based on feature similarity, then routes them to dedicated Modulated Expert (MoE) modules for feature filtering and aggregation according to the condition type. This design eliminates the need for separate preprocessing modules for each condition type, thereby reducing parameter redundancy. Furthermore, to bridge the semantic gap between global visual representations of the base model and local spatial representations from the conditional control units, caused by their independent processing, we propose the WeaveNet architecture. By employing a streamlined serpentine data flow, WeaveNet effectively integrates prompt-guided global semantic constraints with condition image-guided local spatial constraints, enhancing their interaction and significantly mitigating discrepancies arising from separately

processing prompts and conditional images. To validate the effectiveness of our approach, we conduct experiments on the MultiGen-20M [16] and Subjects-200K [13] datasets. Compared to both traditional and latest methods, our approach achieves superior performance across multiple evaluation metrics, with only a slight performance gap in certain metrics compared to methods built upon the FLUX [5] base model.

The main contributions of this paper are summarized as follows:

- A unified generative framework, dubbed **UniGen**, is proposed to support controllable image synthesis under arbitrary types of conditional inputs.
- The **Condition Modulated Expert (CoMoE)** module is proposed to capture both the differences and commonalities among various types of conditional visual representations. It aggregates highly similar token-level features into dedicated expert modules for efficient information fusion, thereby reducing parameter redundancy and computational overhead.
- The **WeaveNet** architecture is proposed to model the dynamic interaction between the global visual information guided by text and the local spatially visual information from the conditional image, addressing the semantic gap and inconsistent representation caused by independently processing global and local visual cues.

## 2 Related Works

Controllable image generation aims to guide image synthesis by jointly leveraging conditional images and textual prompts. Early methods (e.g., [8]) align spatial features by injecting condition information via parallel branches into the main network. Unicontrol [10] employs a Mixture-of-Experts (MoE)-like architecture [17, 18] that selects pretrained embedding layers based on the condition type to achieve feature alignment. Recent works leverage FLUX [5] as a strong backbone, fine-tuning it with LoRA [15] modules for different condition types (e.g., [13, 12, 14]). Despite their effectiveness, these approaches often require training separate LoRA or ControlNet modules or adding parallel branches, which increases model size and complexity, and limits generalization. Moreover, handling each condition independently introduces redundant parameters and overlooks potential shared representations across different conditions. To address these challenges, this paper analyzes the commonalities and distinctions among visual representations of different condition types and proposes an approach that aggregates similar features using independent modules to reduce redundant computation. Additionally, an interactive injection strategy is introduced to align globally text-guided visual features with locally condition-guided features, thereby bridging the semantic gap between them.

## 3 Method

To better support visual control under diverse conditional inputs and enable a unified image-to-image generation framework, we propose UniGen. As illustrated in Fig. 1, UniGen accommodates image generation guided by any of 12 types of conditional inputs. During training, it follows the computational framework of existing image-to-image generation methods [13, 10] and performs conditional noise prediction using a Flow Matching-based [19] approach. First, to address the computational and parameter redundancy caused by existing methods that employ parallel and independent modules for different condition types, we introduce the Condition Modulation Expert (CoMoE) module. As shown in Fig. 2, we leverage the commonalities and differences across diverse condition types to guide expert module selection based on the similarity between patch representations. For patches within the same condition type, we independently process the similar representations of foreground regions, aiming to minimize parameter redundancy. Second, to tackle the lack of effective interaction between global visual representations guided by text and local spatial visual representations guided by conditional images, we introduce the WeaveNet architecture. As illustrated in Fig. 3b, WeaveNet enhances interactive control between text and conditional images through a staggered serpentine computation flow, mitigating local semantic discrepancies and inconsistencies.

### 3.1 Condition Modulated Experts (CoMoE)

To fully exploit the diversity and consistency among various types of conditional visual representations while reducing computational and parameter redundancy, we propose a Conditional Modulation Expert (CoMoE) module. As illustrated in Fig. 2, inspired by the design of Mixture of Experts (MoE) commonly used in large multimodal models [20, 21], the module is composed of independent experts and shared experts. The independent experts are designed to capture common foreground information within the same type of conditional representations, enabling joint representation learning of conditional semantics and visual features for condition-specific visual preprocessing. The shared experts focus on integrating global visual representations guided by textual prompts with local conditional visual features, ensuring consistency between condition information and prompt guidance while reducing their semantic gap.

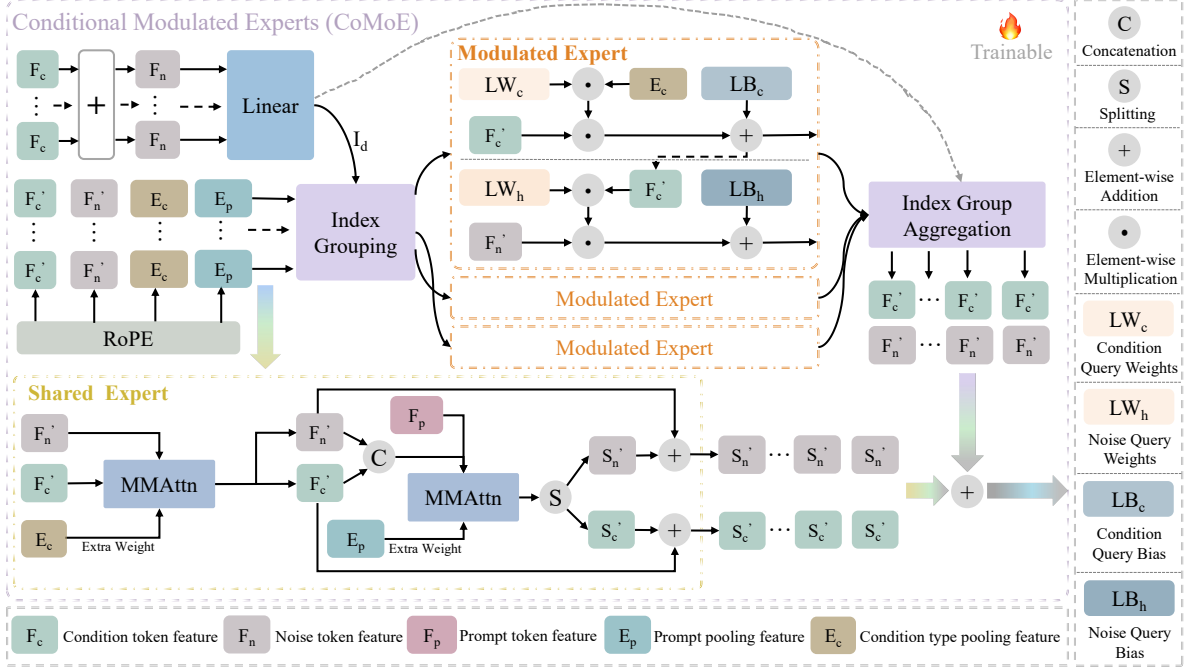


Figure 2: The architecture of Condition Modulated Experts (CoMoE) Module.

**Modulated Expert** First, to address representation ambiguity, information loss, and misalignment caused by certain sparsely structured visual conditions (e.g., Canny, HED, HEDSketch), we introduce a text-guided global visual feature  $F_n$ . By fusing the global representation  $F_n$  with the condition-specific representation  $F_c$ , we jointly determine the selection of independent expert modules, allowing better control over the denoising direction, as shown in Equation 1. Both  $F_n$  and  $F_c$  are preprocessed by a VAE [22] and then converted into token-level visual representations using patch embedding. During training, noise is added to the encoded visual representations  $F_n$  with a strength factor  $\sigma$  as follows:  $F_n = \sigma \cdot N + (1 - \sigma) \cdot F_n$ , where  $N$  denotes the noise. During inference,  $F_n = N$  is used directly as the input to the diffusion model.

$$\begin{cases} S_e = \text{Linear}(F_n + F_c), \\ I_d = \text{Max}(S_e, \text{dim} = -1) \end{cases} \quad (1)$$

In the above equation,  $S_e$  denotes the expert scores predicted by fusing global visual representations with condition-specific visual representations.  $I_d$  represents the indices of expert modules assigned to different patch tokens based on these scores. Guided by these indices, each expert module independently processes foreground regions with higher feature similarity, while background regions are grouped and handled by a separate expert module.

Secondly, to address the loss and misalignment of spatial information caused by Modulated Expert modules processing patch features at the token level, we incorporate Rotary Positional Encoding (RoPE) [23] to embed spatial cues into visual features. In the Modulated Expert module, we aim to leverage condition-specific semantics to process localized visual representations and fuse them with spatially aligned, text-guided global visual features. Specifically, we construct a learnable parameter matrix  $LW_c$ , and extract the semantic representation  $E_c$  based on the category of the given condition. The condition-aware semantic embedding is then used to modulate the parameter matrix, enabling one distinct matrix per condition for conditional feature representation, as shown in Equation 2.

$$\begin{cases} F_n' = \text{RoPE}(F_n), F_c' = \text{RoPE}(F_c), \\ E_c = \text{Pooling}(\text{CLIP}([condition\_types])), \\ LW_c \sim \mathcal{N}(0, 0.1^2), F_c' = LW_c \cdot E_c \cdot F_c', \\ LB_c \sim \mathcal{N}(0, 0.1^2), F_c' = F_c' + LB_c \end{cases} \quad (2)$$

Meanwhile, to further enhance the ability of condition-specific visual representations to constrain the global visual features guided by prompts, we follow the same design principle. A learnable parameter matrix  $LW_h$  is constructed



and modulated using the preprocessed conditional visual feature  $F'_c$  in Equation 2 to reconstruct the feature mapping parameters. This modulation allows control over the effective regions of the global visual representation. During this process, the use of rotary position encoding ensures strict spatial alignment between the representations, thereby avoiding spatial information confusion.

$$\begin{cases} LW_h \sim \mathcal{N}(0, 0.1^2), F'_n = LW_h \cdot F'_c \cdot F'_n, \\ LB_h \sim \mathcal{N}(0, 0.1^2), F'_n = F'_n + LB_h \end{cases} \quad (3)$$

Finally, after aligning the visual representation of the condition with the global visual representation guided by the prompt, each output from the modulated experts corresponds to the same spatial location and semantic type. This alignment effectively enhances the constraint imposed by the condition on the global visual representation. Therefore, we perform reverse aggregation based on the visual token indices  $I_d$  computed in Equation 1 to reconstruct the original ordered distribution of visual tokens.

$$\begin{cases} \hat{F}_n \sim \text{Zero}(F_n), \hat{F}_c \sim \text{Zero}(F_c), \\ \hat{F}_n = \text{Reverse}(F'_n, \hat{F}_n, I_d), \hat{F}_c = \text{Reverse}(F'_c, \hat{F}_c, I_d) \end{cases} \quad (4)$$

In the above equation, *Reverse* refers to reordering the same-type visual representations computed by the Modulated Expert based on the index  $I_d$  obtained from Equation 1, thereby restoring the original distribution of image tokens.

**Shared Expert** The shared expert module leverages a traditional Multi-Modal Attention(MMAttention) mechanism to achieve conditional image generation from two perspectives: one guided by the condition’s visual representation for directional denoising, and the other by the prompt for global denoising. First, the visual representation of the condition is enhanced by encoding its semantic embedding  $E_c$  together with the selected diffusion timestep, which serves as a basis for feature filtering and scaling. Then, attention is used to compute the feature correlation between the condition’s visual features  $F_c$  and the prompt-guided global representation  $F_n$ , thereby reinforcing the influence of the condition in the global visual context. Finally, an attention mechanism is employed to enhance the correlation between local regions within the visual representation of the condition.

$$\begin{cases} T_n = \text{Embedding}(\text{timestep}, E_c), \\ S_n, S_c = \text{MMAttention}(\text{RoPE}(F_n), \text{RoPE}(F_c), T_n), \\ S_c = \text{MMAttention}(S_c, S_c, T_n) \end{cases} \quad (5)$$

In the above equation, embedding layer jointly encodes the pooled features of the condition and the timestep, and the resulting embeddings serve as input to the MMAttention module for computing the offset and scale of the attention-refined features.

Furthermore, to better integrate the joint constraints of conditional visual representations and text prompts, we adopt a similar design strategy as described above to implement the shift and scale operations in the MMAttention module. Meanwhile, we employ text prompts to refine both global and condition-specific visual representations, ensuring accurate instruction adherence under each representation. Through the use of an attention mechanism, the prompt not only guides the global visual representation but also influences the condition representation, thereby avoiding the independence constraint between the prompt and condition representations, as shown in Equation 6.

$$\begin{cases} T'_n = \text{Embedding}(\text{timestep}, E_p), \\ S'_n, S'_c = \text{MMAttention}([\text{RoPE}(F_n), \text{RoPE}(F_c)], F_p, T'_n), \\ S'_n, S'_c = \text{MMAttention}([S'_n, S'_c], [S'_n, S'_c], T'_n), \\ S'_n = S_n + S'_n, S'_c = S_c + S'_c \end{cases} \quad (6)$$

In the above equation,  $[\cdot, \cdot]$  denotes the token-level concatenation of features.  $F_p$  denotes the semantic representation of the prompt encoded by CLIP [24] and T5 [25].

Finally, we aggregate the condition-aware visual representations computed from both the Modulated Expert and the Shared Expert, and also combine the globally constrained visual representations of the condition to enhance spatial-level feature consistency.

$$\begin{cases} \hat{F}_n = \hat{F}_n + S'_n, \\ \hat{F}_c = \hat{F}_c + S'_c, \end{cases} \quad (7)$$

### 3.2 WeaveNet

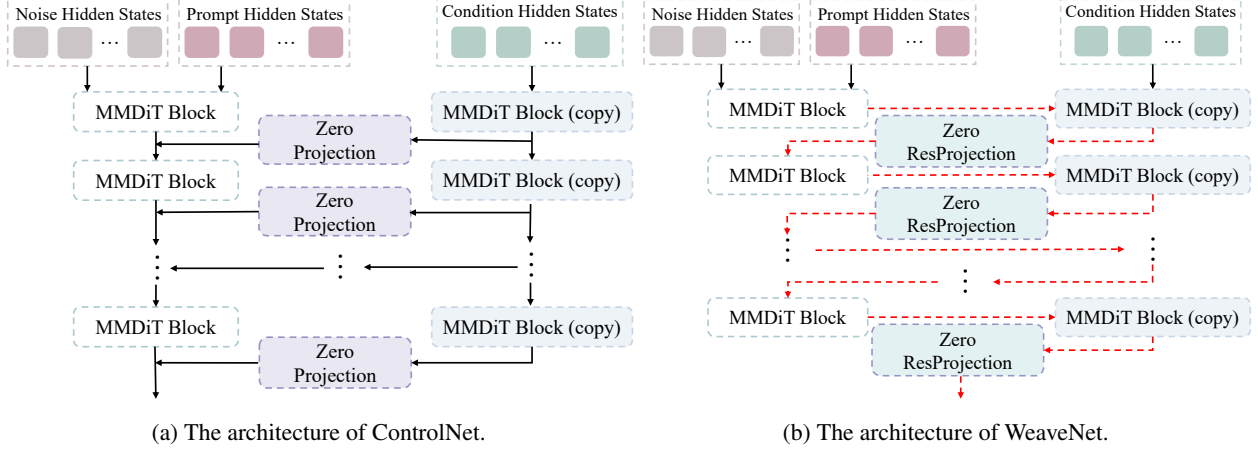


Figure 3: (a) illustrates the structure of the traditional ControlNet, while (b) shows our proposed WeaveNet architecture, which performs conditional control in an interwoven manner. The Zero ResProjection module, initialized with zeros, is a residual network designed to fuse the noise-injected visual representation with the conditional representation.

To address the semantic gap between textual prompts and conditional visual control introduced by existing methods such as ControlNet [8], which processes conditional visual features and textual guidance in parallel via independent branches, we propose a novel architecture named WeaveNet. As illustrated in Fig. 3b, WeaveNet introduces an interactive conditional information injection mechanism that enables dynamic interaction between conditional visual representations and text-guided visual features. Specifically, following the architectural design of ControlNet, we replicate the modules and parameters of the base model to construct a separate branch for processing conditional inputs. Unlike ControlNet, WeaveNet integrates features from the base model into the corresponding layers of the control branch, effectively combining the global semantics from textual prompts with the local information from conditional images. Then, the Zero ResProjection Module is employed to align the outputs of each layer in the control branch and inject them into the main network, ensuring dynamic interaction between the prompt and the conditional image. This helps prevent semantic gaps caused by overemphasis on either side. The detailed computational process is presented in Algorithm 1.

**Algorithm 1** The computational workflow of the WeaveNet architecture.

---

```

1: init WeaveBlocks = copy(DiTBlocks)
2: init  $F_n, F_c$  {Noisy visual features and Conditioned visual features obtained via VAE-based encoding}
3: init  $F_p, E_c, E_p$  { $F_p$  denotes the semantic embedding representation of the prompt, while  $E_c$  and  $E_p$  represent the pooled semantic embeddings of the condition type and the prompt, respectively.}
4: for index in range(len(DiTBlocks)) do
5:    $F_n = \text{DiTBlocks}[\textit{index}](F_n, F_p, E_p)$ 
6:   if index is 0 then
7:      $\hat{F}_n, \hat{F}_c = \text{CoMoE}(F_n, F_c, E_c, E_p, F_p)$ 
8:      $\hat{F}_n = \hat{F}_n + \hat{F}_c$ 
9:      $\hat{F}_n = \text{WeaveBlocks}[\textit{index}](\hat{F}_n, F_p, E_c)$ 
10:   else
11:      $\hat{F}_n = \text{WeaveBlocks}[\textit{index}](F_n, F_p, E_c)$ 
12:   end if
13:    $F_n = F_n + \text{ZeroProjection}(\hat{F}_n)$ 
14: end for
15: return  $F'_n = \text{Reshape}(\text{Projection}(F_n))$ 

```

---

## 4 Experiments

### 4.1 Datasets

We conduct training and evaluation on the MultiGen-20M [16] and Subjects-200K [13] datasets. MultiGen-20M contains over 2 million image-description pairs with corresponding conditional images. These conditional images cover 12 types of conditions, such as depth, Canny edges, OpenPose, HED, normals, and grayscale. However, due to significant inconsistencies in the descriptions constructed for each image in the dataset and generally low annotation accuracy, we re-annotated the entire dataset using Qwen [26] for model training and evaluation. Subjects-200K consists of over 200,000 high-quality images paired with detailed entity annotations and accurate textual descriptions, offering higher image fidelity and more precise captions compared to MultiGen-20M. To further enrich Subjects-200K, we generate conditional images using Dwpose [27] (for OpenPose), Depth Anything [28] (for depth), and Canny [29] operator (for edge maps). For both datasets, we randomly sample 5,000 image-description-condition triplets to construct the test set. We will upload the newly annotated data and test set information to Hugging Face in the future.

### 4.2 Evaluation Metrics

We adopt several widely used evaluation metrics in related work: FID [30], SSIM [31], CLIP-I [32, 24], CLIP-T [32, 24], and DINO [33]. FID evaluates the realism and distributional similarity between generated and real images at the feature level by extracting features using Inception V3 [34]. SSIM measures the similarity between two images in terms of luminance, contrast, and structural information. CLIP-I and CLIP-T leverage CLIP to extract visual and semantic representations. The quality of the generated images is assessed by computing feature similarity between generated and real images (CLIP-I), as well as between generated images and text prompts (CLIP-T). DINO also extracts visual features and measures the semantic structural similarity between generated and real images.

### 4.3 Implement Details

We adopt Stable Diffusion 3.5 Medium [4]<sup>2</sup> as the base model and initialize it with publicly available pretrained weights. The training framework is implemented using PyTorch Lightning and conducted on 8 A100 GPUs with the standard Distributed Data Parallel (DDP) strategy. No compression or acceleration techniques such as DeepSpeed [35] or FSDP [36] are employed.

During training, we use the AdamW [37] optimizer with a learning rate of 0.0001, a constant learning rate scheduler with 500 warm-up steps, and a batch size of 16. This work aims to enhance the model’s adaptability to various conditioning types. To this end, we optimize the distributed sampler to prevent batches from containing samples of the same conditioning type, which could bias the model’s optimization direction. Similar to other reproduced methods, we randomly sample 160,000 condition-description pairs for each conditioning type from the training set.

For evaluation, we follow the same testing protocol as other reproduced models by randomly sampling 5,000 condition-description pairs per conditioning type from the test set. Inference is performed on a single A100 GPU with a condition scale of 1.0, guidance scale of 3.5, and 28 inference steps. Considering the substantial impact of random seeds on sampling outcomes, we fix the seed to 1872 for all experiments. For potential training-free performance improvements, we suggest exploring the impact of different seeds to assess their adaptability across various prompts.

### 4.4 Comparison with state-of-the-art Methods

We train and evaluate our method on Subjects-200K [13] and MultiGen-20M [16]. For fairness, we remove all test samples and randomly sample 160K instruction–target–condition image triplets per condition from the remaining data for training. We compare against traditional baselines like UniControl [10] and ControlNet++ [16], as well as recent state-of-the-art methods such as OminiControl [13] and PixelPonder [11]. Unlike OminiControl, which is built on FLUX [5], our method is based on Stable Diffusion [4].

First, as shown in Table 1, we conduct comparative evaluations on the Subjects-200K and MultiGen-20M datasets under three conditioning types: Depth, Canny, and OpenPose. It is evident that our method achieves significant improvements over existing approaches across all metrics, including SSIM, FID, CLIP-I, and DINO. Moreover, the average performance across different conditions for the same metric consistently reaches the best results. This demonstrates that our approach not only enables effective and high-quality controllable image generation but also exhibits strong generalization capabilities, achieving significant gains across various input conditions. Second, for the nine additional conditions in the MultiGen-20M dataset, as shown in Table 2, our method achieves top or near-top

<sup>2</sup><https://huggingface.co/stabilityai/stable-diffusion-3.5-medium>

Metrics	Method	Condition Type							
		Subjects-200K				MultiGen-20M			
		Depth	Canny	Openpose	Mean	Depth	Canny	Openpose	Mean
SSIM $\uparrow$	UniControl [10]	0.33	0.42	0.24	0.33	0.19	0.19	0.19	0.19
	UniControl ++ [16]	0.39	0.41	-	0.4	0.28	0.28	-	0.28
	OminiControl $\dagger$ [13]	<u>0.49</u>	<b>0.58</b>	<u>0.33</u>	<u>0.47</u>	<b>0.34</b>	<b>0.43</b>	<u>0.25</u>	<u>0.34</u>
	PixelPonder $\dagger$ [11]	0.35	0.39	<u>0.33</u>	0.36	0.28	0.33	<u>0.25</u>	0.27
	<b>UniGen(ours)</b>	<b>0.5</b>	<b>0.55</b>	<b>0.39</b>	<b>0.48</b>	<b>0.34</b>	<b>0.43</b>	<b>0.28</b>	<b>0.35</b>
FID $\downarrow$	UniControl [10]	23.34	18.23	36.69	26.09	57.63	57.31	57.84	57.59
	UniControl ++ [16]	15.99	23.26	-	19.63	<u>22.24</u>	37.56	-	<u>29.9</u>
	OminiControl $\dagger$ [13]	<u>12.35</u>	<b>9.38</b>	35.03	<u>18.92</u>	22.92	<u>15.34</u>	52.0	30.09
	PixelPonder $\dagger$ [11]	24.11	21.86	30.98	25.65	24.83	20.92	65.94	37.23
	<b>UniGen(ours)</b>	<b>11.26</b>	<b>9.52</b>	<b>15.68</b>	<b>12.15</b>	<b>13.45</b>	<b>11.83</b>	<b>15.43</b>	<b>13.57</b>
CLIP-I $\uparrow$	UniControl [10]	84.95	87.99	77.80	83.58	64.49	64.53	64.47	64.50
	UniControl ++ [16]	87.04	86.75	-	86.90	73.86	72.83	-	73.35
	OminiControl $\dagger$ [13]	<b>90.59</b>	<b>93.13</b>	<u>79.84</u>	<b>87.85</b>	<u>75.05</u>	<u>82.73</u>	64.9	<u>74.23</u>
	PixelPonder $\dagger$ [11]	79.98	83.35	76.89	80.07	74.17	79.50	<u>67.64</u>	73.77
	<b>UniGen(ours)</b>	<u>89.14</u>	<u>91.61</u>	<b>82.72</b>	<u>87.82</u>	<b>76.77</b>	<b>84.06</b>	<b>71.54</b>	<b>77.46</b>
CLIP-T $\uparrow$	UniControl [10]	18.49	18.24	19.18	18.64	19.23	19.54	19.38	19.38
	UniControl ++ [16]	18.83	19.36	-	19.10	19.33	19.95	-	19.64
	OminiControl $\dagger$ [13]	19.96	20.58	<u>20.59</u>	20.38	19.16	19.53	19.91	19.53
	PixelPonder $\dagger$ [11]	<b>21.56</b>	<b>21.75</b>	<b>21.4</b>	<b>21.57</b>	<b>20.62</b>	<b>20.63</b>	<b>20.19</b>	<b>20.48</b>
	<b>UniGen(ours)</b>	19.51	20.21	20.55	20.09	<u>19.56</u>	<u>20.06</u>	<b>20.19</b>	<u>19.94</u>
DINO $\uparrow$	UniControl [10]	91.23	92.35	82.28	88.62	75.72	<u>75.75</u>	75.69	75.72
	UniControl ++ [16]	93.02	91.0	-	92.0	87.99	85.96	-	<u>86.98</u>
	OminiControl $\dagger$ [13]	<b>95.42</b>	<b>96.14</b>	<u>85.94</u>	<u>92.5</u>	<u>88.39</u>	<u>92.1</u>	<u>79.14</u>	86.54
	PixelPonder $\dagger$ [11]	86.03	88.97	82.79	85.93	84.78	88.48	76.22	83.16
	<b>UniGen(ours)</b>	<u>94.31</u>	<u>95.20</u>	<b>88.11</b>	<b>92.54</b>	<b>88.68</b>	<b>92.19</b>	<b>83.74</b>	<b>88.20</b>

Table 1: We conduct a comprehensive performance comparison under Depth, Canny, and OpenPose conditions using the Subjects-200K and MultiGen-20M datasets.  $\dagger$  denotes the use of FLUX [5] as the base model.

performance across multiple evaluation metrics. These results indicate that our approach not only ensures accurate conditional control and high image quality but also maintains strong generalization across different condition types. At the same time, we observe that our method performs relatively weaker on the CLIP-T metric. This is primarily because the proposed WeaveNet architecture reduces the reliance on prompts during conditional control. Consequently, compared to approaches that use independent branches for prompt-based global generation, our method may be less efficient at aligning image content with textual instructions, leading to suboptimal CLIP-T scores. Finally, we analyze model parameters and inference time. As shown in Table 3, traditional ControlNet [8] architectures introduce significant parameter redundancy and increased inference time as the number of condition types grows. Although OmniControl trains separate LoRA modules on top of FLUX for each condition type and avoids drastic parameter increases, its total parameter count is still several times larger than ours. This helps explain its relatively strong performance under certain conditions or metrics. Overall, our method not only maintains a compact parameter size but also achieves lower inference overhead.

#### 4.5 Ablation Studies

To comprehensively validate the effectiveness of each module, we conducted an extensive ablation study from five perspectives: the impact of the WeaveNet architecture, the roles of the Modulated Expert and Rotary Position Embedding (RoPE), the necessity of the Shared Expert, and the influence of the number of experts and conditional control layers. First, as shown in Table 4, the WeaveNet architecture significantly outperforms the original ControlNet across all three conditions in terms of SSIM, FID, CLIP-I, and DINO metrics. We also observe a slight decline in the CLIP-T metric, which is primarily due to the WeaveNet architecture potentially weakening the influence of text on the image, as it balances the joint constraints of textual and conditional visual information. Second, regarding the effectiveness of the Modulated Expert, Table 5 shows that the first row represents the conventional MoE [17, 18] design, which uses a multilayer perceptron (MLP) to process and map features. Compared to the configuration combining Modulated Expert and RoPE, there is a significant performance gap in pixel-level image generation. This indicates that using a standard MLP to handle sparsely distributed conditional visual information fails to provide precise control signals, leading to a

Metric	Method	Condition Types									Mean
		Hed	Hedsketch	Normal	Seg	Bbox	Outpainting	Inpainting	Blur	Grayscale	
SSIM $\uparrow$	UniControl	0.19	0.19	0.19	0.19	0.19	0.19	0.19	0.19	0.19	0.19
	UniControl ++	0.20	-	-	-	-	-	-	-	-	-
	OminiControl <sup>†</sup>	<u>0.41</u>	<u>0.36</u>	<u>0.36</u>	<u>0.30</u>	0.22	<b>0.56</b>	<b>0.77</b>	<u>0.70</u>	<b>0.90</b>	<u>0.51</u>
	PixelPonder <sup>†</sup>	0.33	0.32	0.29	0.27	<u>0.25</u>	0.41	0.57	0.57	0.68	0.41
	<b>UniGen(ours)</b>	<b>0.45</b>	<b>0.41</b>	<b>0.37</b>	<b>0.31</b>	<b>0.26</b>	<b>0.56</b>	<b>0.76</b>	<b>0.73</b>	<b>0.90</b>	<b>0.53</b>
FID $\downarrow$	UniControl	57.51	57.55	57.81	57.78	57.72	57.79	57.78	57.87	57.88	57.74
	UniControl ++	46.07	-	-	-	-	-	-	-	-	-
	OminiControl <sup>†</sup>	<u>12.59</u>	<u>20.08</u>	<u>19.56</u>	33.51	67.10	<u>11.50</u>	<b>7.46</b>	<u>8.21</u>	<u>7.09</u>	<u>20.79</u>
	PixelPonder <sup>†</sup>	17.26	21.87	24.15	<u>31.24</u>	<u>64.09</u>	19.09	14.96	13.34	11.11	24.12
	<b>UniGen(ours)</b>	<b>8.22</b>	<b>12.42</b>	<b>12.64</b>	<b>14.19</b>	<b>16.26</b>	<b>9.69</b>	<b>7.72</b>	<b>7.21</b>	<b>6.77</b>	<b>10.57</b>
CLIP-I $\uparrow$	UniControl	64.50	64.49	64.48	64.48	64.48	64.55	64.54	64.54	64.53	64.51
	UniControl ++	72.49	-	-	-	-	-	-	-	-	-
	OminiControl <sup>†</sup>	<u>82.25</u>	<u>79.1</u>	<u>78.27</u>	69.30	62.29	<b>88.43</b>	<b>93.33</b>	<b>97.38</b>	<b>94.32</b>	<u>82.74</u>
	PixelPonder <sup>†</sup>	79.98	78.61	75.49	<u>71.67</u>	<u>67.71</u>	80.65	85.53	89.89	91.75	80.14
	<b>UniGen(ours)</b>	<b>84.06</b>	<b>81.01</b>	<b>79.96</b>	<b>73.23</b>	<b>69.52</b>	<u>87.60</u>	<u>92.52</u>	<u>96.88</u>	<u>94.15</u>	<b>84.33</b>
CLIP-T $\uparrow$	UniControl	18.85	18.45	19.06	19.31	19.08	18.98	19.56	19.26	18.75	19.03
	UniControl ++	19.73	-	-	-	-	-	-	-	-	-
	OminiControl <sup>†</sup>	18.65	18.25	19.21	19.22	19.35	19.06	19.18	18.91	19.10	18.99
	PixelPonder <sup>†</sup>	<b>20.0</b>	<b>19.59</b>	<b>20.49</b>	<b>20.61</b>	<b>20.12</b>	<b>21.13</b>	<b>21.0</b>	<b>20.53</b>	<b>21.05</b>	<b>20.50</b>
	<b>UniGen(ours)</b>	<u>19.30</u>	<u>18.70</u>	<u>19.80</u>	<u>19.99</u>	<u>19.76</u>	<u>19.66</u>	<u>19.58</u>	<u>19.53</u>	<u>19.28</u>	<u>19.51</u>
DINO $\uparrow$	UniControl	75.72	75.72	75.70	75.70	75.70	75.71	75.71	75.70	75.70	75.71
	UniControl ++	86.22	-	-	-	-	-	-	-	-	-
	OminiControl <sup>†</sup>	<u>92.07</u>	<u>90.13</u>	<u>90.41</u>	83.78	75.10	<b>93.38</b>	<b>97.47</b>	<b>98.20</b>	<b>98.57</b>	<u>91.01</u>
	PixelPonder <sup>†</sup>	89.33	88.07	86.06	81.44	<u>76.31</u>	88.24	93.5	95.54	97.06	88.39
	<b>UniGen(ours)</b>	<b>92.50</b>	<b>90.66</b>	<b>90.72</b>	<b>85.44</b>	<b>81.11</b>	<u>92.97</u>	<u>96.85</u>	<u>97.86</u>	<u>98.41</u>	<b>91.84</b>

Table 2: Comparison with state-of-the-art image-to-image conditional control models on the MultiGen-20M test set. <sup>†</sup> denotes the use of FLUX [5] as the base model.

Condition Nums	Method	Params(B) $\downarrow$	Inference Times $\downarrow$
3	ControlNet	6.03	58.12
	OminiControl	11.93	13.06
	<b>UniGen</b>	<b>4.1</b>	<b>6.82</b>
12	ControlNet	17.38	59.16
	OminiControl	12.07	15.74
	<b>UniGen</b>	<b>4.69</b>	<b>13.96</b>

Table 3: Complexity analysis between ControlNet, OminiControl and UniGen.

noticeable decline in overall image reconstruction quality. Furthermore, the introduction of RoPE brings a substantial performance improvement by preserving relative spatial position information, which is often lost when processing token-level visual representations in MoE-based architectures. This effectively strengthens local conditional control. Third, regarding the Shared Expert module, as shown in Table 6, introducing the shared expert module improves FID by 1.05. Fourth, concerning the number of Modulated Experts, Table 7 shows that performance is optimal when the number of conditional experts reaches six, enabling the generation of higher-quality images. Finally, regarding the number of control layers, as illustrated in Fig. 4, both excessively deep and shallow configurations lead to significant performance degradation. Optimal generation quality is achieved when the number of control layers is set to 12.

Con.	Me.	SSIM $\uparrow$	FID $\downarrow$	CLIP-I $\uparrow$	CLIP-T $\uparrow$	DINO $\uparrow$
Depth	CN	<b>0.49</b>	12.6	88.72	<b>20.81</b>	93.9
	WN	<b>0.49</b>	<b>11.26</b>	<b>89.02</b>	18.28	<b>94.31</b>
Canny	CN	<b>0.55</b>	10.34	91.31	<b>21.27</b>	94.88
	WN	<b>0.55</b>	<b>9.52</b>	<b>91.53</b>	19.26	<b>95.2</b>
Openpose	CN	0.37	16.36	82.21	<b>20.93</b>	87.54
	WN	<b>0.38</b>	<b>15.68</b>	<b>82.40</b>	19.40	<b>88.11</b>

Table 4: Comparison of ControlNet and WeaveNet under different conditional settings on the Subjects-200K test set.

Module	SSIM $\uparrow$	FID $\downarrow$	CLIP-I $\uparrow$	CLIP-T $\uparrow$	DINO $\uparrow$
-	0.48	11.82	88.83	<b>20.63</b>	94.09
w. MoE	<b>0.50</b>	11.71	88.96	20.60	94.08
w. MoE/RoPE	0.49	<b>11.26</b>	<b>89.02</b>	18.28	<b>94.31</b>

Table 5: Ablation study on the effectiveness of the Modulated Expert (MoE) and Rotational Position Encoding (RoPE).

Shared Expert	SSIM $\uparrow$	FID $\downarrow$	CLIP-I $\uparrow$	CLIP-T $\uparrow$	DINO $\uparrow$
$\times$	0.49	12.31	88.75	<b>20.14</b>	93.70
$\checkmark$	0.49	<b>11.26</b>	<b>89.02</b>	18.28	<b>94.31</b>

Table 6: Ablation study on the effectiveness of the Shared Expert.

Expert Numbers	SSIM $\uparrow$	FID $\downarrow$	DINO $\uparrow$
2	0.49	11.80	94.28
3	<b>0.50</b>	11.90	94.17
4	0.49	11.72	94.25
6	0.49	<b>11.26</b>	<b>94.31</b>
8	0.49	11.74	94.20
9	0.48	12.02	94.01
10	0.48	11.66	94.11
12	0.48	11.72	94.20

Table 7: Ablation study on the number of Modulated Expert modules.

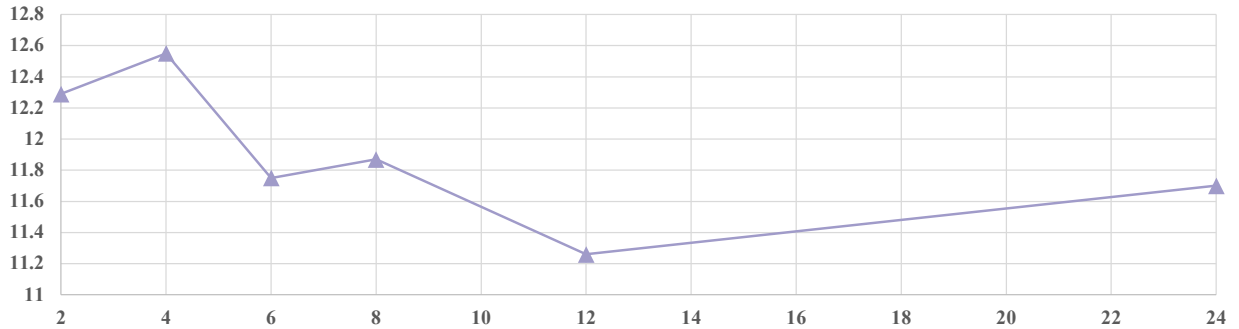


Figure 4: Ablation study on the number of conditional control layers in WeaveNet.

#### 4.6 Qualitative Analysis

As shown in Fig. 5, we compare our method with OmniControl under two types of conditions: Depth and OpenPose. Under the simpler Depth condition, our method demonstrates stronger instruction adherence and better alignment with the overall semantic content of the prompt. Under the more challenging OpenPose condition, our approach effectively captures the task-relevant information while maintaining visual quality and prompt consistency. Additional visualizations and comparisons are provided in Appendix.

## 5 Conclusion

This paper proposes a Unified Generative framework, UniGen, designed to handle various types of conditional image-guided generation tasks in a consistent manner. First, we introduce the Condition Modulated Expert (CoMoE) module, which enables unified processing of multiple condition types, effectively reducing computational and parameter redundancy caused by designing separate modules for each condition. Second, we present the WeaveNet architecture, which integrates global semantics from prompt guidance with local spatial information from conditional images, addressing semantic misalignment and enhancing both local consistency and overall image quality. Experimental results demonstrate that UniGen achieves superior performance across multiple datasets and evaluation metrics, validating its effectiveness and generality in image-to-image generation tasks.



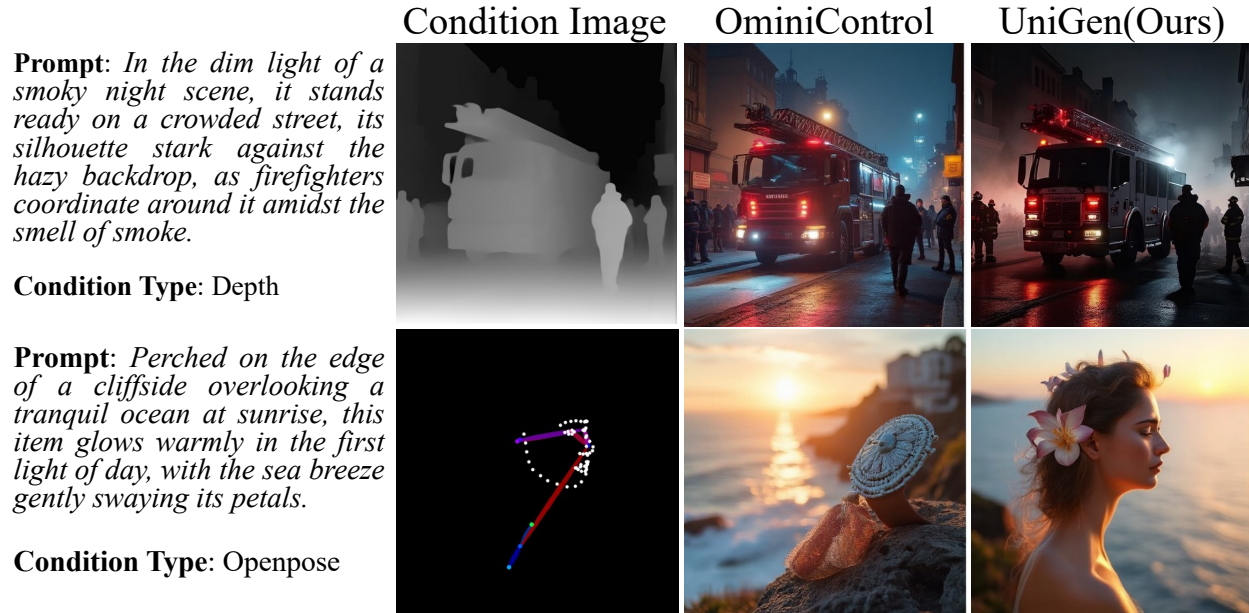


Figure 5: Comparison with OmniControl on Conditional Image Generation

## References

- [1] Jonathan Ho, Ajay Jain, and Pieter Abbeel. Denoising diffusion probabilistic models. *Advances in neural information processing systems*, 33:6840–6851, 2020.
- [2] Alexander Quinn Nichol and Prafulla Dhariwal. Improved denoising diffusion probabilistic models. In *International conference on machine learning*, pages 8162–8171. PMLR, 2021.
- [3] Robin Rombach, Andreas Blattmann, Dominik Lorenz, Patrick Esser, and Björn Ommer. High-resolution image synthesis with latent diffusion models. In *Proceedings of the IEEE/CVF conference on computer vision and pattern recognition*, pages 10684–10695, 2022.
- [4] Patrick Esser, Sumith Kulal, Andreas Blattmann, Rahim Entezari, Jonas Müller, Harry Saini, Yam Levi, Dominik Lorenz, Axel Sauer, Frederic Boesel, et al. Scaling rectified flow transformers for high-resolution image synthesis. In *Forty-first international conference on machine learning*, 2024.
- [5] Black Forest Labs. Flux. <https://github.com/black-forest-labs/flux>, 2024.
- [6] Olaf Ronneberger, Philipp Fischer, and Thomas Brox. U-net: Convolutional networks for biomedical image segmentation. In *International Conference on Medical image computing and computer-assisted intervention*, pages 234–241. Springer, 2015.
- [7] William Peebles and Saining Xie. Scalable diffusion models with transformers. In *Proceedings of the IEEE/CVF international conference on computer vision*, pages 4195–4205, 2023.
- [8] Lvmin Zhang, Anyi Rao, and Maneesh Agrawala. Adding conditional control to text-to-image diffusion models. In *Proceedings of the IEEE/CVF international conference on computer vision*, pages 3836–3847, 2023.
- [9] Hu Ye, Jun Zhang, Sibio Liu, Xiao Han, and Wei Yang. Ip-adapter: Text compatible image prompt adapter for text-to-image diffusion models. *arXiv preprint arXiv:2308.06721*, 2023.
- [10] Can Qin, Shu Zhang, Ning Yu, Yihao Feng, Xinyi Yang, Yingbo Zhou, Huan Wang, Juan Carlos Niebles, Caiming Xiong, Silvio Savarese, et al. Unicontrol: A unified diffusion model for controllable visual generation in the wild. *arXiv preprint arXiv:2305.11147*, 2023.
- [11] Yanjie Pan, Qingdong He, Zhengkai Jiang, Pengcheng Xu, Chaoyi Wang, Jinlong Peng, Haoxuan Wang, Yun Cao, Zhenye Gan, Mingmin Chi, et al. Pixelponder: Dynamic patch adaptation for enhanced multi-conditional text-to-image generation. *arXiv preprint arXiv:2503.06684*, 2025.
- [12] Haoxuan Wang, Jinlong Peng, Qingdong He, Hao Yang, Ying Jin, Jiafu Wu, Xiaobin Hu, Yanjie Pan, Zhenye Gan, Mingmin Chi, et al. Unicombe: Unified multi-conditional combination with diffusion transformer. *arXiv preprint arXiv:2503.09277*, 2025.



- [13] Zhenxiong Tan, Songhua Liu, Xingyi Yang, Qiaochu Xue, and Xinchao Wang. Ominicontrol: Minimal and universal control for diffusion transformer. *arXiv preprint arXiv:2411.15098*, 2024.
- [14] Yuxuan Zhang, Yirui Yuan, Yiren Song, Haofan Wang, and Jiaming Liu. Easycontrol: Adding efficient and flexible control for diffusion transformer. *arXiv preprint arXiv:2503.07027*, 2025.
- [15] Edward J Hu, Yelong Shen, Phillip Wallis, Zeyuan Allen-Zhu, Yuanzhi Li, Shean Wang, Lu Wang, Weizhu Chen, et al. Lora: Low-rank adaptation of large language models. *ICLR*, 1(2):3, 2022.
- [16] Ming Li, Taojiannan Yang, Huafeng Kuang, Jie Wu, Zhaoning Wang, Xuefeng Xiao, and Chen Chen. Controlnet++: Improving conditional controls with efficient consistency feedback: Project page: liming-ai. github.io/controlnet\_plus\_plus. In *European Conference on Computer Vision*, pages 129–147. Springer, 2024.
- [17] Noam Shazeer, Azalia Mirhoseini, Krzysztof Maziarczyk, Andy Davis, Quoc Le, Geoffrey Hinton, and Jeff Dean. Outrageously large neural networks: The sparsely-gated mixture-of-experts layer. *arXiv preprint arXiv:1701.06538*, 2017.
- [18] William Fedus, Barret Zoph, and Noam Shazeer. Switch transformers: Scaling to trillion parameter models with simple and efficient sparsity. *Journal of Machine Learning Research*, 23(120):1–39, 2022.
- [19] Yaron Lipman, Ricky TQ Chen, Heli Ben-Hamu, Maximilian Nickel, and Matt Le. Flow matching for generative modeling. *arXiv preprint arXiv:2210.02747*, 2022.
- [20] Bin Lin, Zhenyu Tang, Yang Ye, Jiaxi Cui, Bin Zhu, Peng Jin, Jinfa Huang, Junwu Zhang, Yatian Pang, Munan Ning, et al. Moe-llava: Mixture of experts for large vision-language models. *arXiv preprint arXiv:2401.15947*, 2024.
- [21] Ziteng Wang, Jun Zhu, and Jianfei Chen. Remoe: Fully differentiable mixture-of-experts with relu routing. *arXiv preprint arXiv:2412.14711*, 2024.
- [22] Diederik P Kingma, Max Welling, et al. Auto-encoding variational bayes, 2013.
- [23] Jianlin Su, Murtadha Ahmed, Yu Lu, Shengfeng Pan, Wen Bo, and Yunfeng Liu. Roformer: Enhanced transformer with rotary position embedding. *Neurocomputing*, 568:127063, 2024.
- [24] Alec Radford, Jong Wook Kim, Chris Hallacy, Aditya Ramesh, Gabriel Goh, Sandhini Agarwal, Girish Sastry, Amanda Askell, Pamela Mishkin, Jack Clark, et al. Learning transferable visual models from natural language supervision. In *International conference on machine learning*, pages 8748–8763. PmLR, 2021.
- [25] Colin Raffel, Noam Shazeer, Adam Roberts, Katherine Lee, Sharan Narang, Michael Matena, Yanqi Zhou, Wei Li, and Peter J Liu. Exploring the limits of transfer learning with a unified text-to-text transformer. *Journal of machine learning research*, 21(140):1–67, 2020.
- [26] Jinze Bai, Shuai Bai, Yunfei Chu, Zeyu Cui, Kai Dang, Xiaodong Deng, Yang Fan, Wenbin Ge, Yu Han, Fei Huang, Binyuan Hui, Luo Ji, Mei Li, Junyang Lin, Runji Lin, Dayiheng Liu, Gao Liu, Chengqiang Lu, Keming Lu, Jianxin Ma, Rui Men, Xingzhang Ren, Xuancheng Ren, Chuanqi Tan, Sinan Tan, Jianhong Tu, Peng Wang, Shijie Wang, Wei Wang, Shengguang Wu, Benfeng Xu, Jin Xu, An Yang, Hao Yang, Jian Yang, Shusheng Yang, Yang Yao, Bowen Yu, Hongyi Yuan, Zheng Yuan, Jianwei Zhang, Xingxuan Zhang, Yichang Zhang, Zhenru Zhang, Chang Zhou, Jingren Zhou, Xiaohuan Zhou, and Tianhang Zhu. Qwen technical report. *arXiv preprint arXiv:2309.16609*, 2023.
- [27] Zhendong Yang, Ailing Zeng, Chun Yuan, and Yu Li. Effective whole-body pose estimation with two-stages distillation. In *Proceedings of the IEEE/CVF International Conference on Computer Vision*, pages 4210–4220, 2023.
- [28] Lihe Yang, Bingyi Kang, Zilong Huang, Zhen Zhao, Xiaogang Xu, Jiashi Feng, and Hengshuang Zhao. Depth anything v2. *Advances in Neural Information Processing Systems*, 37:21875–21911, 2024.
- [29] John Canny. A computational approach to edge detection. *IEEE Transactions on pattern analysis and machine intelligence*, (6):679–698, 1986.
- [30] Martin Heusel, Hubert Ramsauer, Thomas Unterthiner, Bernhard Nessler, and Sepp Hochreiter. Gans trained by a two time-scale update rule converge to a local nash equilibrium. *Advances in neural information processing systems*, 30, 2017.
- [31] Zhou Wang, Alan C Bovik, Hamid R Sheikh, and Eero P Simoncelli. Image quality assessment: from error visibility to structural similarity. *IEEE transactions on image processing*, 13(4):600–612, 2004.
- [32] Jack Hessel, Ari Holtzman, Maxwell Forbes, Ronan Le Bras, and Yejin Choi. Clipscore: A reference-free evaluation metric for image captioning. *arXiv preprint arXiv:2104.08718*, 2021.

- [33] Mathilde Caron, Hugo Touvron, Ishan Misra, Hervé Jégou, Julien Mairal, Piotr Bojanowski, and Armand Joulin. Emerging properties in self-supervised vision transformers. In *Proceedings of the IEEE/CVF international conference on computer vision*, pages 9650–9660, 2021.
- [34] Christian Szegedy, Vincent Vanhoucke, Sergey Ioffe, Jon Shlens, and Zbigniew Wojna. Rethinking the inception architecture for computer vision. In *Proceedings of the IEEE conference on computer vision and pattern recognition*, pages 2818–2826, 2016.
- [35] Jeff Rasley, Samyam Rajbhandari, Olatunji Ruwase, and Yuxiong He. Deepspeed: System optimizations enable training deep learning models with over 100 billion parameters. In *Proceedings of the 26th ACM SIGKDD international conference on knowledge discovery & data mining*, pages 3505–3506, 2020.
- [36] Samyam Rajbhandari, Olatunji Ruwase, Jeff Rasley, Shaden Smith, and Yuxiong He. Zero-infinity: Breaking the gpu memory wall for extreme scale deep learning. In *Proceedings of the international conference for high performance computing, networking, storage and analysis*, pages 1–14, 2021.
- [37] Ilya Loshchilov and Frank Hutter. Decoupled weight decay regularization. *arXiv preprint arXiv:1711.05101*, 2017.
- [38] Zhimin Li, Jianwei Zhang, Qin Lin, Jiangfeng Xiong, Yanxin Long, Xinchu Deng, Yingfang Zhang, Xingchao Liu, Minbin Huang, Zedong Xiao, Dayou Chen, Jiajun He, Jiahao Li, Wenyue Li, Chen Zhang, Rongwei Quan, Jianxiang Lu, Jiabin Huang, Xiaoyan Yuan, Xiaoxiao Zheng, Yixuan Li, Jihong Zhang, Chao Zhang, Meng Chen, Jie Liu, Zheng Fang, Weiyan Wang, Jinbao Xue, Yangyu Tao, Jianchen Zhu, Kai Liu, Sihuan Lin, Yifu Sun, Yun Li, Dongdong Wang, Mingtao Chen, Zhichao Hu, Xiao Xiao, Yan Chen, Yuhong Liu, Wei Liu, Di Wang, Yong Yang, Jie Jiang, and Qinglin Lu. Hunyuan-dit: A powerful multi-resolution diffusion transformer with fine-grained chinese understanding, 2024.

## A Qualitative Analysis

### A.1 Comparative Analysis of Image Generation Quality

Firstly, we conduct a visual comparative analysis of generation quality based on the Subjects-200K dataset. As shown in the Fig. 6, we present results conditioned on Depth, Canny, and Openpose. In Fig. 6, it is evident that under relatively simple conditions such as Depth and Canny, the difference in generation quality between OminiControl and our method is minimal. However, in finer details—for example, under Depth conditioning—OminiControl tends to overfit to the structural information of the condition image while neglecting the holistic semantic background described in the prompt.

In contrast, for the more challenging and sparse Openpose condition, OminiControl exhibits significant issues in local detail generation. For instance, in the last row, the spatial structure of the legs is incorrectly generated. We further extend the visual comparison to the MultiGen-20M dataset across nine additional conditioning types. As illustrated in Fig. 7, under BBox, Normal, and Outpainting conditions, our method more effectively follows both the visual guidance from the condition input and the semantic cues from the prompt, producing more accurate and higher-quality results compared to OminiControl. Particularly in the Outpainting task, our method generates more precise extensions while maintaining global image consistency.

Furthermore, under the Hed, Hedskech, and Seg conditions (Fig. 8), the difference is less pronounced for relatively simpler conditions like Hed and Hedskech. Nonetheless, our method provides richer detail. Notably, even under sparse guidance from Hedskech, our model maintains strong instruction adherence and condition control, delivering more accurate and higher-quality results (e.g., fourth row). For the more complex and noisy Seg conditions, our method continues to produce accurate and high-quality images.

Finally, for Inpainting, Blur, and Grayscale tasks (Fig. 9), our method consistently generates more accurate and visually appealing results. Specifically, in the Inpainting task, the content generated within the masked region shows high consistency with surrounding context, yielding more natural and aesthetic outcomes. As Blur and Grayscale conditions typically offer more precise and dense control signals than other tasks, the generated outputs across different models appear generally similar in overall structure. However, differences emerge in fine-grained details and color fidelity. Under Blur conditions, our method generates sharper details, while under Grayscale conditions, it produces colorizations that are more realistic and aesthetically pleasing.

To further assess the robustness of our method, we compare it with HunyuanDiT [38], a state-of-the-art open-source model. Using the official released weights<sup>3</sup>, we evaluate conditional generation quality under Depth, Canny, and Openpose settings. As shown in Fig. 10, HunyuanDiT often suffers from loss of control signals. In sparse conditioning

<sup>3</sup><https://github.com/Tencent-Hunyuan/HunyuanDiT>



Figure 6: Based on the Subjects-200K dataset, we conduct a comprehensive comparison with UniControl [10] and OminiControl [13] under Depth, Canny, and OpenPose conditions.

scenarios such as Openpose, it tends to either lose key information or overfit the condition input, resulting in reduced global consistency and the appearance of unrealistic "fake" elements, ultimately degrading the authenticity of the generated images.

## A.2 Visualization of Image Generation Results

We present the generation results for all 12 conditions using the test sets of Subjects-200K and MultiGen-20M. As shown in Fig. 11 - 15, the generated images under various conditional images and textual instructions are illustrated. Overall, our method enables controllable image generation by effectively leveraging visual cues from conditional images and guidance from textual prompts, while ensuring high realism and visual quality.



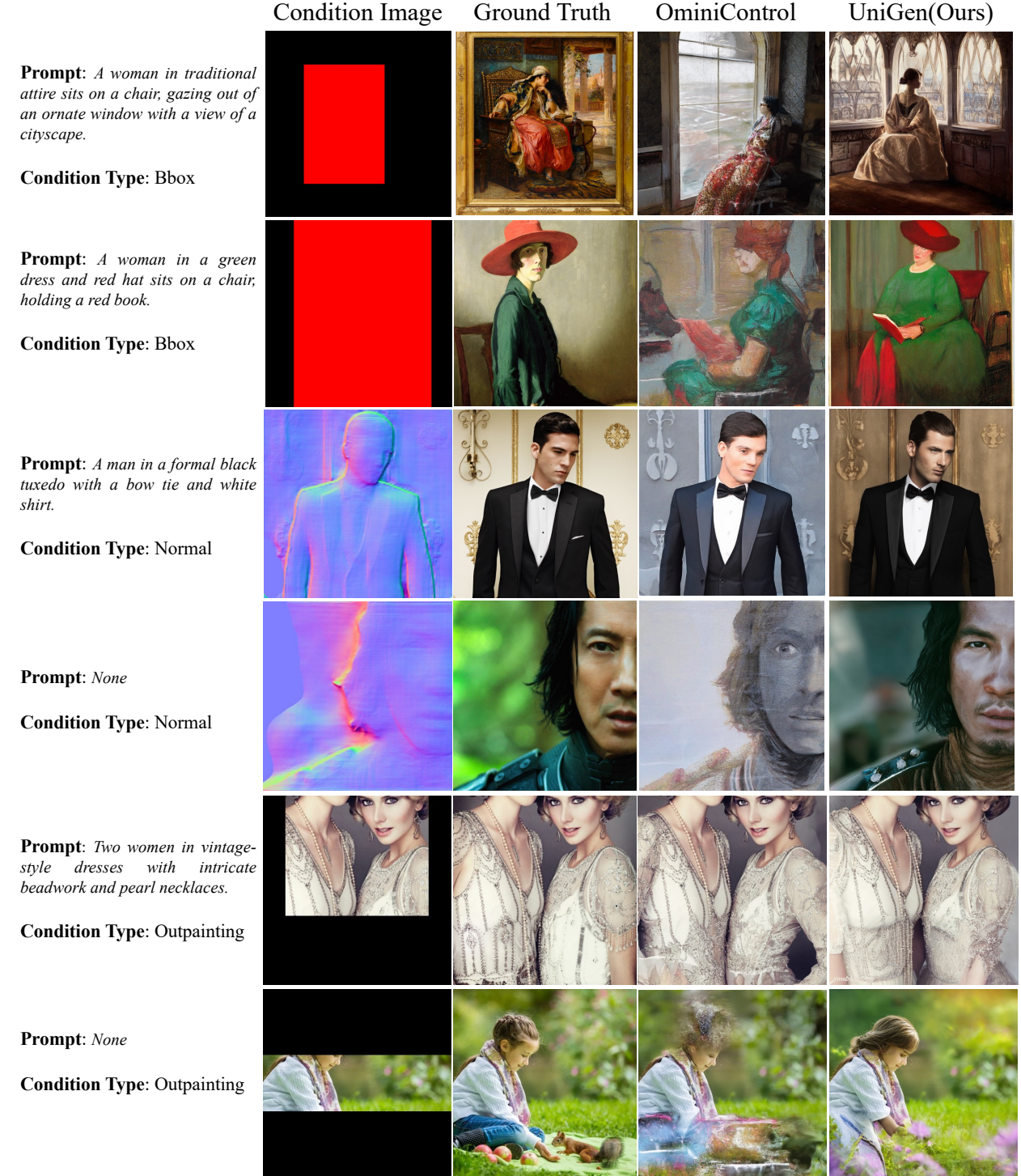


Figure 7: Based on the MultiGen-20M dataset, we conduct a comprehensive comparison with OminiControl [13] under Bbox, Normal, and Outpainting conditions.



Figure 8: Based on the MultiGen-20M dataset, we conduct a comprehensive comparison with OminiControl [13] under Hed, Hedsketch, and Seg conditions.





Figure 9: Based on the MultiGen-20M dataset, we conduct a comprehensive comparison with OminiControl [13] under Inpainting, Blur, and Grayscale conditions.

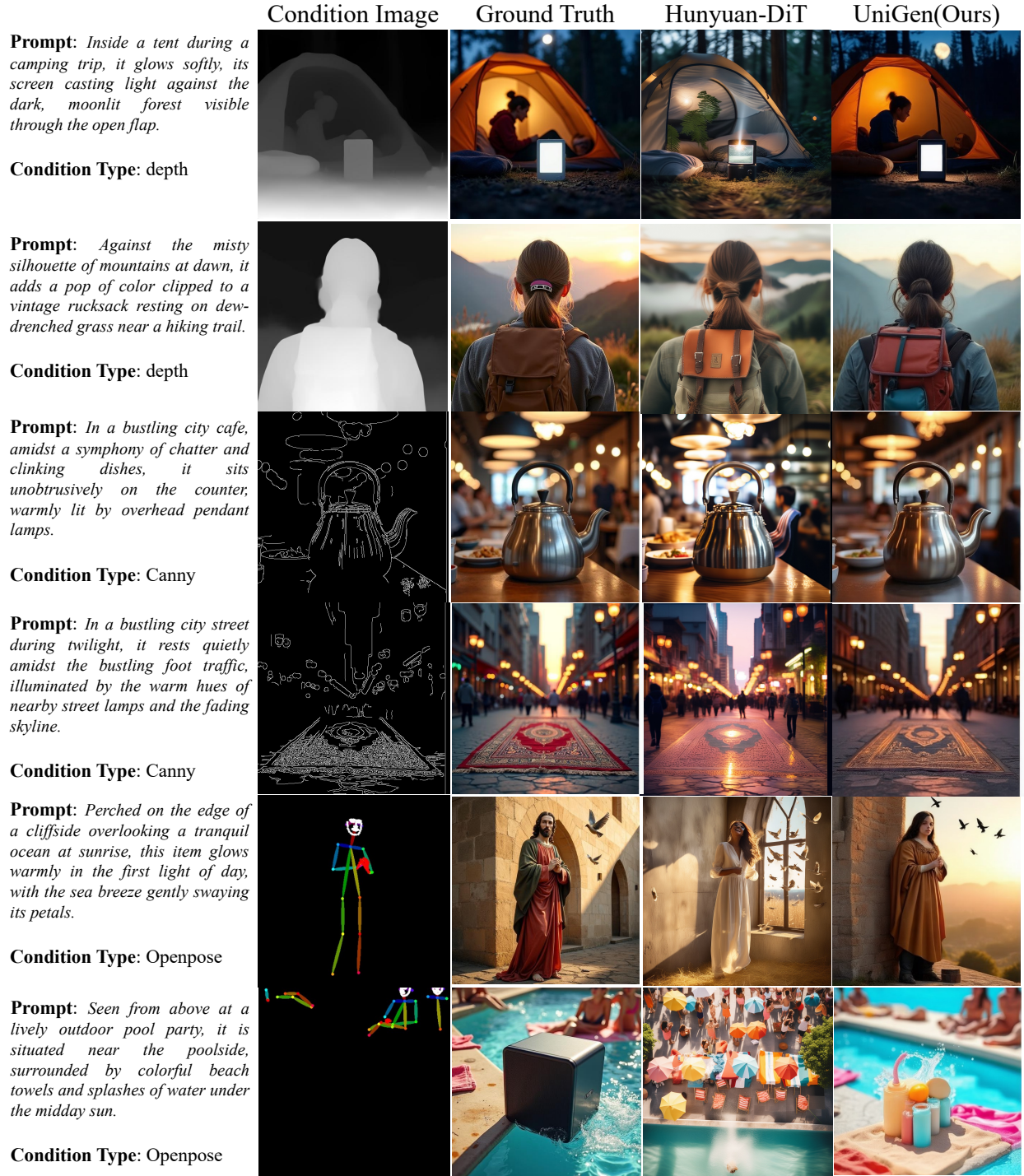


Figure 10: Based on the Subjects-200K dataset, we conduct a comprehensive comparison with HunyuanDiT [38] under Depth, Canny, and OpenPose conditions.



# Condition Weaving Meets Expert Modulation: Towards Universal and Controllable Image Generation

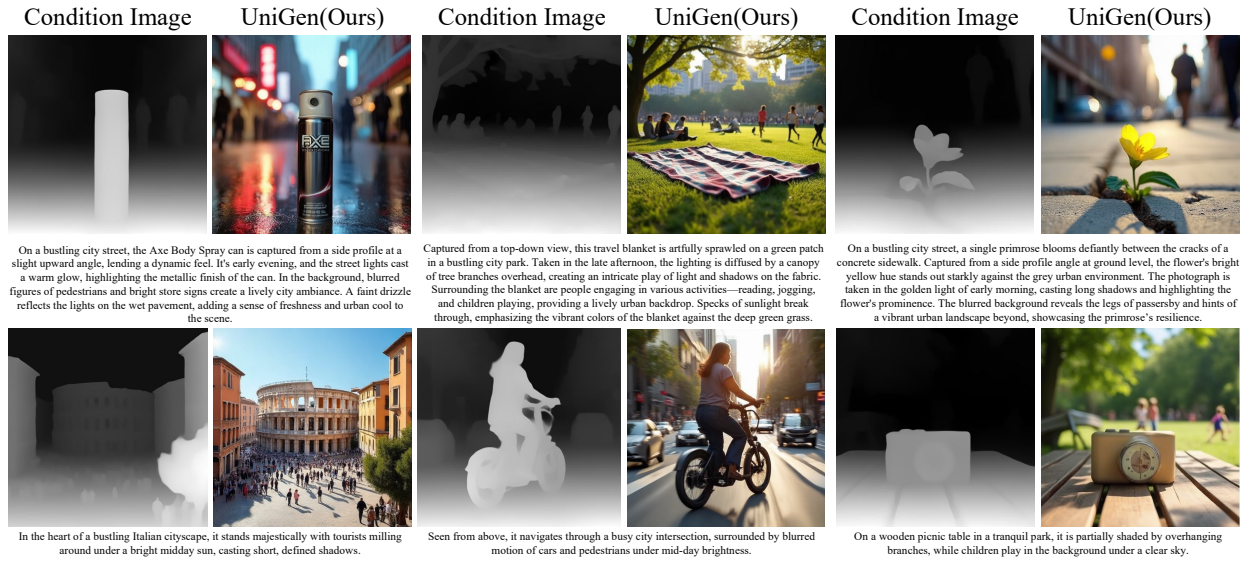


Figure 11: Generation results conditioned on Depth.

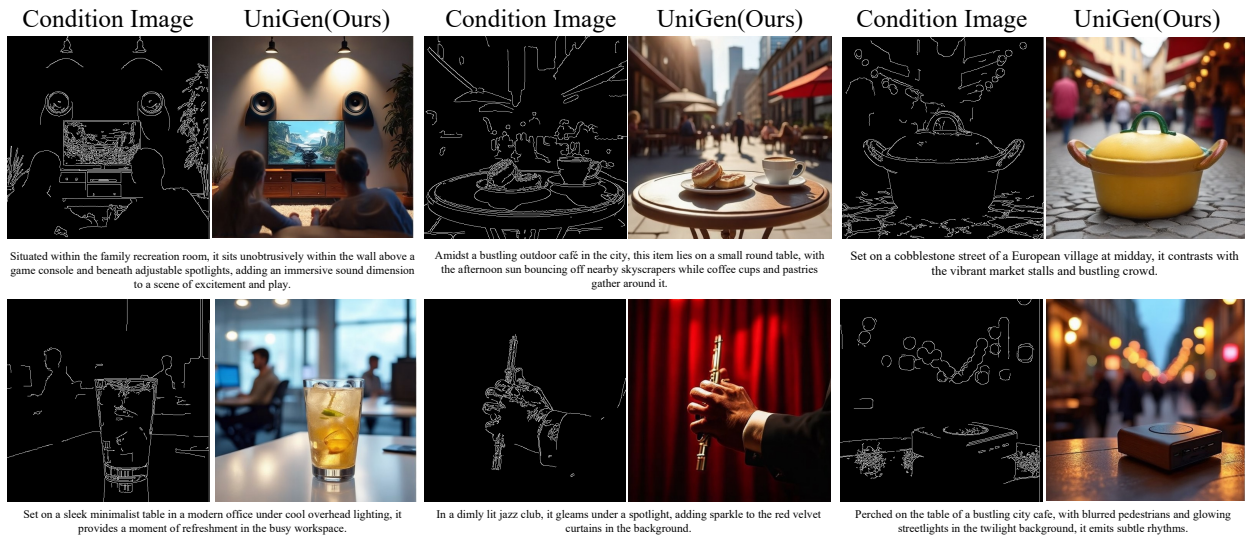


Figure 12: Generation results conditioned on Canny.

## Condition Weaving Meets Expert Modulation: Towards Universal and Controllable Image Generation

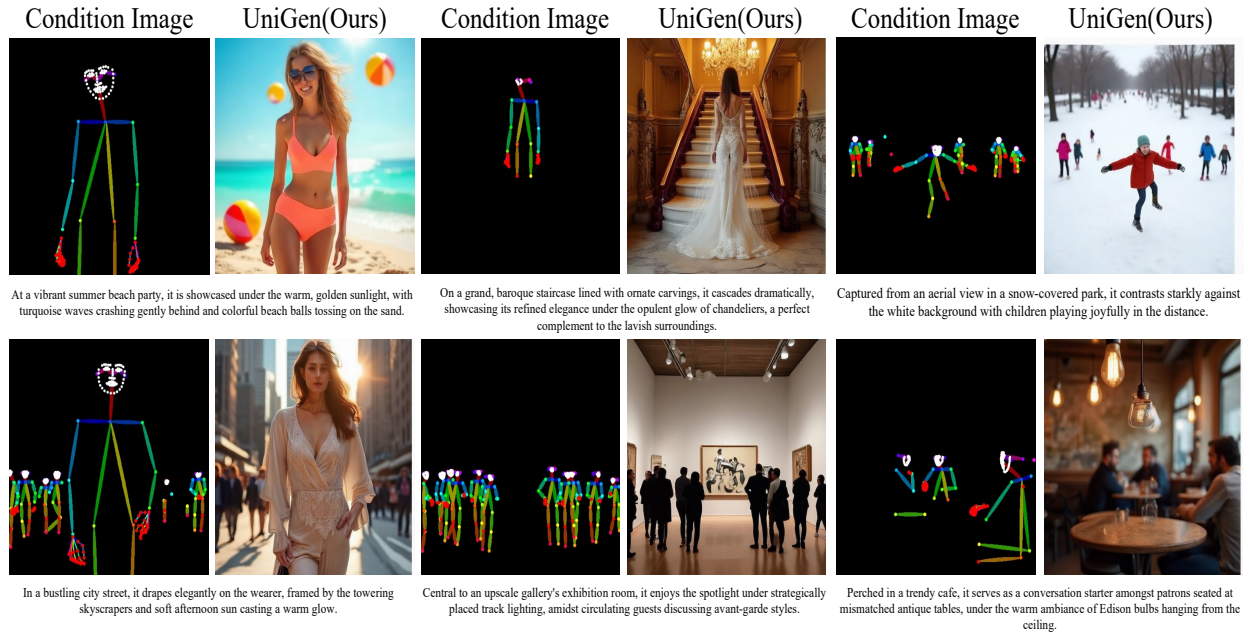


Figure 13: Generation results conditioned on Openpose.

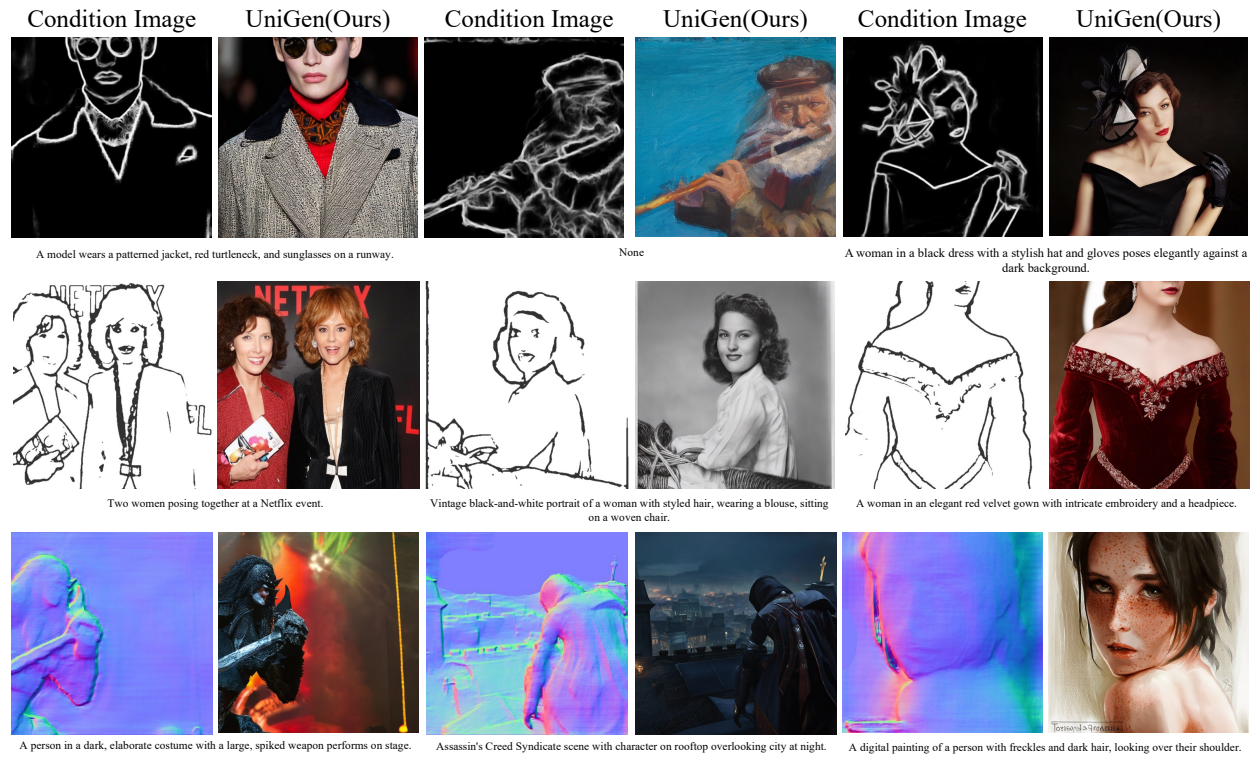


Figure 14: Generation results conditioned on HED, Hedsketch, and Normal.



# Condition Weaving Meets Expert Modulation: Towards Universal and Controllable Image Generation

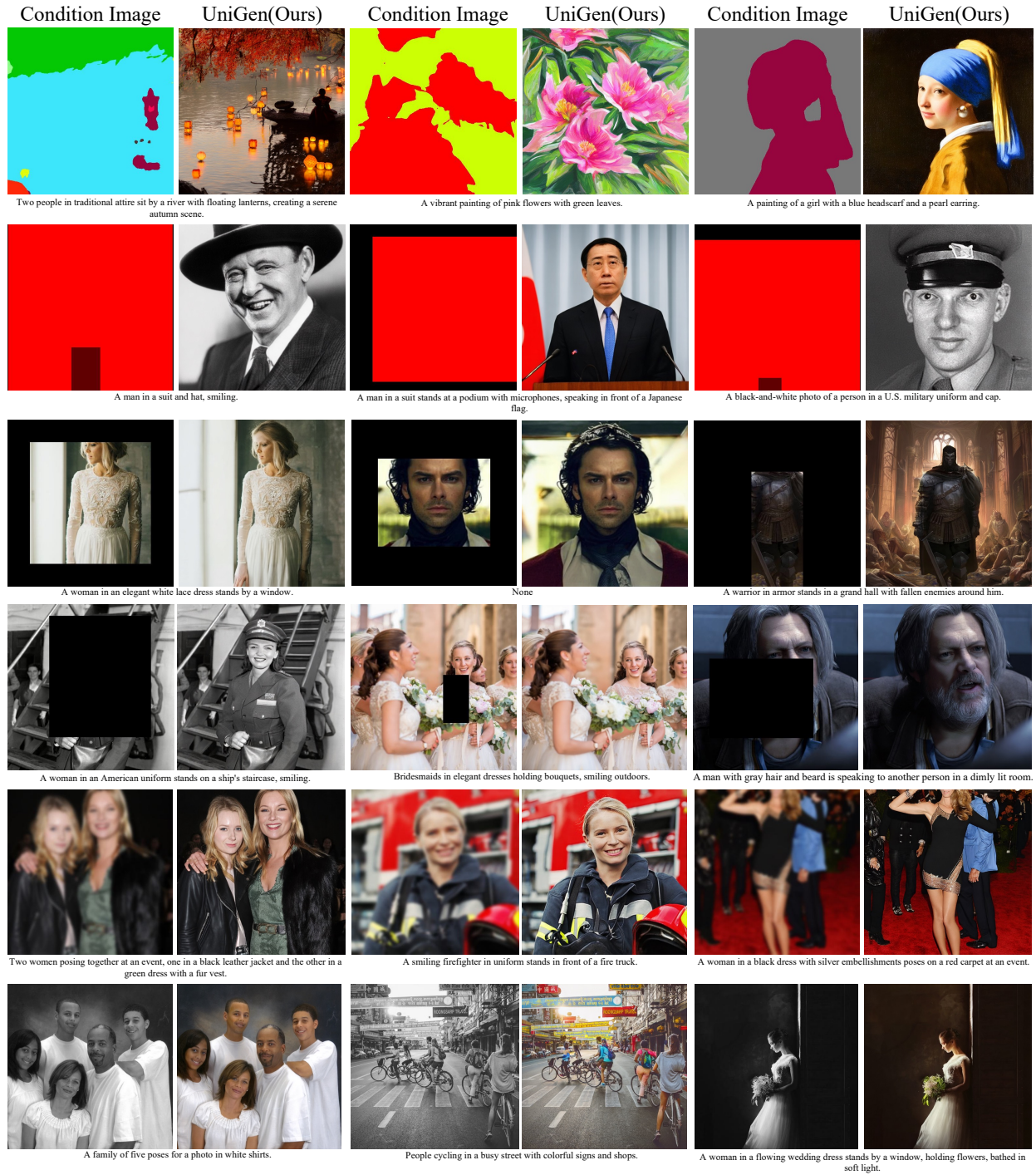


Figure 15: Generation results conditioned on Seg, Bbox, Outpainting, Inpainting, Blur and Grayscale.